Shear Flow-Induced Detachment Kinetics of *Dictyostelium discoideum* Cells from Solid Substrate

Emmanuel Décavé,† Daniel Garrivier,* Yves Bréchet,‡ Bertrand Fourcade,* and Franz Bruckert†

*Département de Recherche Fondamentale sur la Matière Condensée/SI3M, and †Département de Biologie Moléculaire et Structurale/BBSI, Commissariat à l'Energie Atomique Grenoble, 38054 Grenoble cedex 9, and ‡L'Ecole Nationale Supérieure Electrochimie Electrométallurgie, Laboratoire de Thermodynamique et de Physico-Chimie Metallurgiques, Domaine Universitaire, F-38402 Saint Martin d'Hères, France

ABSTRACT Using *Dictyostelium discoideum* as a model organism of specific and nonspecific adhesion, we studied the kinetics of shear flow-induced cell detachment. For a given cell, detachment occurs for values of the applied hydrodynamic stress above a threshold. Cells are removed from the substrate with an apparent first-order rate constant that strongly depends on the applied stress. The threshold stress depends on cell size and physicochemical properties of the substrate, but is not affected by depolymerization of the actin and tubulin cytoskeleton. In contrast, the kinetics of cell detachment is almost independent of cell size, but is strongly affected by a modification of the substrate and the presence of an intact actin cytoskeleton. These results are interpreted in the framework of a peeling model. The threshold stress and the cell-detachment rate measure the local equilibrium energy and the dissociation rate constant of the adhesion bridges, respectively.

INTRODUCTION

In the context of a cellular organism, adhesion is a highly regulated process. Cells are not per se adhesive with respect to each other or to the intracellular matrix because of the presence of a repulsive polymer coating called glycocalyx (Bongrand et al., 1982). The capacity to make specific contacts arises as members of families of adhesion proteins are expressed. Many of these adhesion proteins are also receptors, eliciting a cellular response upon ligand binding. Cellular signaling results in further stabilization of cell contact, as with integrins and cadherins, or to the application of intracellular forces leading to cell motility (Albelda and Buck, 1990; Takeichi, 1990; Hynes 1987).

In the case of *Dictyostelium discoideum*, a unicellular eukaryote also able to complete a pluricellular development cycle, membrane adhesiveness is tightly related to lifestyle. In the vegetative phase, the small (8-μm diameter) ameba feeds upon bacteria and yeast by phagocytosis. Plasma membrane adhesion is therefore directly related to the phagocytic properties of the cell. In the development phase, cell–cell adhesion is more important, and specific contact proteins are expressed (Bozzaro and Ponte, 1995). Axenic strains showing an enhanced fluid-phase endocytosis have been obtained and are able to grow in suspension in nutritive medium (Ashworth and Watts, 1970; Williams et al., 1974). The sequencing of *D. discoideum* 34-Mbp genome and Expressed Sequenced Tags from various developmental stages are currently in a completion phase (Kay and Williams, 1999; Morio et al., 1998). The available molecular tools make *D. discoideum* a good model organism to study phagocytosis and cellular motility using null or overexpression mutants (de Lozanne and Spudich, 1987; Manstein et al., 1995). Several mutant studies suggested the existence of three kinds of adhesion protein. A glucose-selective lectin, mediating attachment of bacteria to the cell, was revealed by the sensitivity of mutants to 50 mM glucose (Vogel et al., 1980). A hydrophilic receptor called Phg1, consisting of a 9-helix transmembrane protein was recently identified (Cornillon et al., 2000). As for now, the molecular nature of its ligand is unknown, but it is present in nutritive media, because Phg1 null mutants are adhesion defective in this medium. The third class of adhesion molecule is sensitive to surface hydrophobicity, as exemplified by the HV32 mutant, which does not bind to polystyrene in the presence of glucose (Vogel et al., 1980; Chia, 1996).

Quantitative measurements of cell–substrate adhesion are difficult because this process involves the collective behavior of individual proteins confined on a two-dimensional membrane geometry. Therefore, measuring cell–substrate adhesion is inseparable from modeling the geometry of the contact zone. Experimentally, applying external forces is required to obtain quantitative information on adhesion strength and relevant mechanical parameters of living cells. Three methods have been used with success. In the first one, individual cells submitted to a weak shear flow, not sufficient to detach them, are imaged. The surface of the contact zone is then reconstructed from optical measurements, and its geometry is interpreted in the frame of Bruinsma's model as detailed in Simson et al., (1998). Three parameters are derived from this analysis: the surface adhesion energy W_{adh}, the bending modulus κ and the surface tension γ of the membrane. These parameters not only reflect the properties of the membrane surface, but also those of the underlying cytoskeleton. A second method uses external forces to detach cells from the substrate as in micropipette (Evans and Leung, 1984), or shear flow experiments (Chan et al.,

Submitted May 7, 2001, and accepted for publication February 7, 2002.

Address reprint requests to Franz Bruckert, DBMS/BBSI, CEA/Grenoble, 17 Rue des Martyrs, F-38054 Grenoble Cedex 9, France. Tel.: +33-4-38-78-54-19; Fax: +33-4-38-78-61-07; E-mail: fbruckert@cea.fr.

0006-3495/02/05/2383/13 $2.00

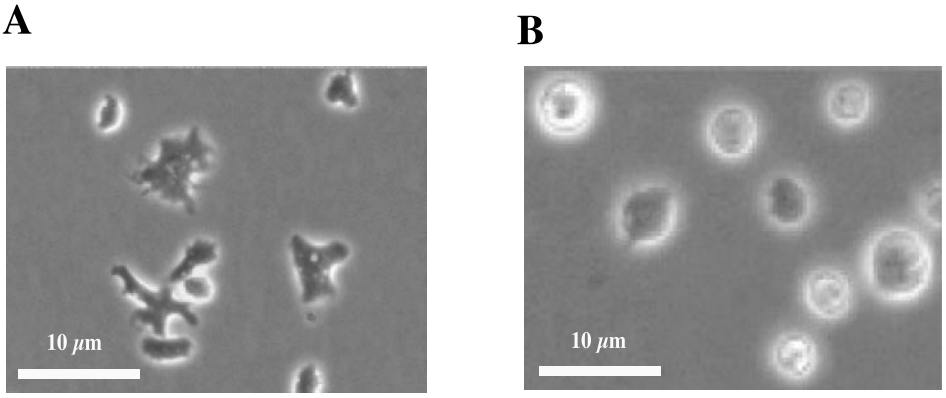

FIGURE 1 Control of cell shape by the actin cytoskeleton. (*A*) Control cells exhibit many pseudopods and filopods. (*B*) CIPC-treated cells, where the actin cytoskeleton has been depolymerized, have a more regular shape.

1991; Cozens-Roberts et al., 1990a). In this case, a model should explain how the mechanical energy associated with the work of the applied forces is dissipated within the cellular structure, creating deformation, and at the cell–surface interface, allowing disruption of the cell–substrate contacts. A new peeling model for shear flow-induced cell detachment was developed in this context (D. Garrivier, E. Decave, Y. Brechet, F. Bruckert, B. Fourcade, submitted for publication). A third method uses rolling of cells on molecularly tailored surfaces to probe the adhesive properties of the membrane surface (Dunon et al., 1996). In this case, the formation of a single molecular bond is sufficient to stop the cell. The statistics of cell halts is directly related to the dissociation rate constant of this bond (Pierres et al., 1994). The major interest of studying rolling is that it allows for elimination of complex cell functions, because rolling may be achieved with fixed cells or even artificial systems.

It should be noted that, in many physiological situations, the most relevant parameters are the cell-detachment kinetics. For instance, the speed of amoeboid movement is limited by the retraction of the lagging pseudopodia (DiMilla et al., 1993; Palecek et al., 1997). The efficiency of phagocytic capture, and the extent of lymphocyte rolling on endothelial cells, in part is limited by the duration of cell–cell contact. These phenomena ultimately depend on the molecular association and dissociation rate constants. It is therefore of great interest to relate cell-detachment kinetics to the molecular receptor–ligand dissociation rate.

In this paper, we study the flow-induced detachment of *D. discoideum* amebas adhering on a flat substrate. Modeling hydrodynamic forces acting on a sphere or on a deformable object near a wall is complex, and partial solutions of this problem have only been obtained in a limited number of cases (Cantat, 1999; Goldman et al., 1967). From an experimental point of view, hydrodynamic forces have, however, the advantage that comparable forces can be applied simultaneously to very large number of cells, obviating the shape and statistical problems. The relative value of these forces is also easily controlled by changing the flow rate. The cells remaining on the substrate can be imaged during the application of forces. Previous work consistently showed that the applied hydrodynamic stress should reach a critical value for the cells to detach. This critical threshold stress was interpreted as the force needed to overcome the surface tension of the membrane due to adhesion (DiMilla et al., 1993; Palecek et al., 1997). This interpretation, based on a theoretical work by Dembo et al. (1988), is, however, not firmly grounded because this equilibrium is always neutral (see D. Garrivier, E. Decave, Y. Brechet, F. Bruckert, B. Fourcade, submitted for publication), and, consequently, does not explain the presence of a threshold stress of cell detachment.

One of the difficult aspects of cell mechanics is the complex shape cells exhibit. The shape of living cells such as *D. discoideum* amebas spread on a polystyrene Petri dish surface (Fig. 1 *A*) obviously shows that the cell surface should not be considered as uniform. The tips of elongated cell structures are likely to correspond to reinforced adhesion zones. Cell–substrate adhesion should therefore not be described by a continuum, but rather by discrete adhesion bridges. This situation was circumvented by the statistics and by modifying cell shape. Because we measure cell detachment on a large number of cells, the details of individual cells were averaged. However, this does not rule out that some of the adhesion parameters depend on the presence of shape singularities. We used cytoskeleton-disrupting agents to convert *D. discoideum* cells into more symmetrical structures, looking like liposomes (Fig. 1 *B*). Drugs such as cytochalasin A, nocodazole, and *N*-(3-chlorophenyl)-isopropyl-carbamate (CIPC) induce a fast actin or tubulin depolymerization (Aubry, 1994). In the case of *D. discoideum*, where the cell shape is entirely controlled by actin microfilaments and actin-binding proteins, actin depolymerization eliminates pseudopodia and filopodia (de Priester et al., 1988). Under these conditions, we will be able to probe the passive behavior of the cell in contact with

a flat substrate, independently of shape singularities actively created by the structured cytoskeleton.

Combining experimental and theoretical approaches, we want to address three questions. What is the significance of the threshold associated with cell detachment? Which role does the cytoskeleton play in cell–substrate adhesion? How is the adhesion of cells related to the microscopic properties of individual adhesion proteins? Several methods are indeed available to measure the biochemical parameters of receptor–ligand interaction, even under an external force (Pierres et al., 1995, 1996). It remains afterwards to combine this molecular information with the cell mechanics to predict the behavior of living cells. These papers try to fill the gap and provide a conceptual framework to exploit the experimental techniques probing adhesion molecules in their cellular environment.

This paper describes the experimental study of *D. discoideum* detachment in a radial flow chamber. Evidence will be given that the cells detach by a peeling process, and its consequence on the physiological meaning of the various experimental parameters will be derived. Our peeling model of cell detachment is exposed and scaled with the value of the parameters determined in the experimental part in D. Garrivier, E. Decave, Y. Brechet, F. Bruckert, B. Fourcade, submitted for publication (2002). Mathematical relations derived from the theoretical model will be used to fit the data obtained in this paper.

METHODS

Chemicals

N-(3-chlorophenyl)-isopropyl-carbamate (CIPC) and nocodazole were supplied by Sigma (St Louis, MO). Dimethyldichlorosilane (DDS) and aminopropyltriethoxysilane (APS) were supplied by ABCR (Karlsruhe, Germany). Other chemicals were supplied by Prolabo (Lyon, France).

Cell growth and preparation

Ax-2 cells were grown in axenic medium (Ashworth and Watts, 1970) in agitated suspensions (180 rpm). Unless otherwise stated, vegetative cells were harvested during exponential phase at a density of $2–4.10^6$ cells·ml^{-1}, pelleted by centrifugation ($1000 \times g$, 4°C, 4 min) and washed twice in Sörensen phosphate buffer (2 mM Na_2HPO_4/14.5 mM KH_2PO_4, pH = 6.2). Cell pellets (10^7 cells) were stored on ice and used within 8 h, without noticeable change in their adhesion properties. CIPC and nocodazole were dissolved in DMSO at 20 mg/mL.

Substrate surface treatment

Borosilicate glass plates, (Mini Protean II outer glass plates, 105×85 mm^2), were purchased from BioRad (Ivry sur Seine, France), cleaned with a mild detergent, etched for 5 min in a concentrated NaOH solution (14.5 M), thoroughly rinsed with ethanol and distilled water, and dried under a dust-free nitrogen flow. DDS-treated plates were prepared by immersing the clean glass plates in a solution of 5% DDS in toluene for 2 h, with agitation. The DDS-treated plates were then washed with toluene, ethanol, and, finally, distilled water, before being dried at 120°C for 2 h. APS-treated plates were prepared by immersing clean glass plates in a solution of 1% APS in 5 mM aqueous acetic acid for 20 min, with agitation. The APS-treated plates were then washed with distilled water before drying at 100°C for 15 min. Contact angles for H_2O were determined for both types of treated plates, at four points. Measured values (31° for glass, 134° for DDS-treated plate and 95° for APS-treated plate) were similar to those previously reported (Turner et al., 1995; Kamath et al., 1996). The plates were stored in a dessicator at room temperature.

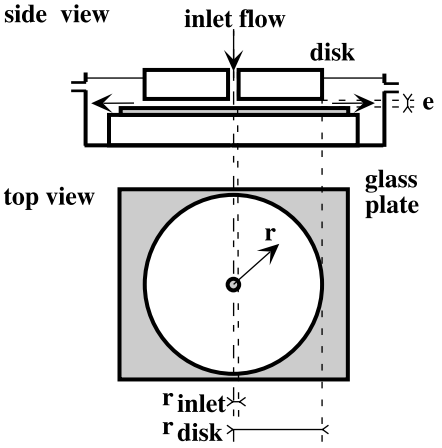

FIGURE 2 Experimental setup. A radial hydrodynamic flow is generated between the stainless steel disk and the glass plate on which cells adhere. The shear stress induced by the flow on the plate decreases as $1/r$.

Cell detachment assay

A radial flow detachment assay was adapted from the setup used by Lauffenburger and coworkers to study cell or bead adhesion to solid substrates (Cozens-Roberts et al., 1990a, 1990b; DiMilla et al., 1993). Cells were resuspended in Sörensen buffer and spread evenly at a density of 300 cells·mm^{-2} on a glass plate whose surface properties were eventually modified by covalent chemistry. The possible influence of collective behavior of cells, resulting from long-range hydrodynamic interaction of cells, was tested by changing the initial cell density on the plate. Identical detachment curves were obtained at 180, 360, or 720 cells·mm^{-2}. Cells therefore behaved independently, provided that the fraction of the surface occupied did not exceed 7%. The cells were allowed to settle for 10–20 min. The whole suspension rested on the plate, retained by the balance between gravity and capillary forces. The settling time was lengthened when hydrophobic plates were used, because the volume of the suspension had to be doubled to cover the entire surface. The invariance in the initial state of cellular adherence was checked. No change in the detachment curve was observed when the settling time was varied from 5 to 20 min. Consequently, as far as detachment is concerned, the initial state of cell adherence can be considered as stable. The plate was then submerged by raising the level of Sörensen buffer contained in the lower tank of the apparatus.

A flat stainless steel disk (80 mm diameter) pierced in its center (1.5 mm orifice diameter) was placed above, taking care not to trap any bubble below. The distance, e, between the disk and the plate (0.21 ± 0.01 mm or 0.56 ± 0.02 mm, depending on the conditions used) was adjusted with three screws using calibrated spacers. The central orifice of the disk was connected to an upper tank filled with Sörensen buffer, and the fluid was allowed to flow by gravity. The fluid levels in the upper and lower tanks were maintained constant by two pumps, permitting a direct measurement of the flow rate. The cells were thus submitted to a shear flow under a controlled laminar radial geometry (see Fig. 2). In this simple geometry,

the velocity field decreases with the distance to the disk orifice. The flow is laminar, as indicated by the value of the Reynolds number, which is always less than 2000.

The action of shear flow on the cell adhering on the substrate is determined by the hydrodynamic forces exerted on the cell. When the forces exerted were sufficient, cells were removed from the solid surface and taken away in the bulk flow. Modeling the cell mechanics under a hydrodynamic field of forces is extremely complex. Nevertheless, when inertial effects can be neglected, the net force and torque exerted by a laminar shear flow on an adhering cell, considered as an elastic solid, are proportional to the wall shear stress σ, i.e., the hydrodynamic stress on the solid substrate in the absence of the cell. In the radial geometry, σ decreases inversely with the distance, r, to the origin of the flow according to

$$\sigma(r) = \frac{3D\eta}{\pi r e^2}, \qquad (1)$$

where D is the flow rate, η is the dynamic viscosity of the fluid, and e the space between disk and plate. In this way, a wide range of stresses can be studied in one single experiment. At a given flow rate, the range of experimentally attainable values for σ is determined by the size of the orifice (region of maximum stress) and the disk diameter (minimum stress). From hydrodynamic considerations, the distance to the origin of the flow necessary for the fluid to obey Poiseuille flow was estimated to be equal to the inlet radius. As for the minimum stress, as the fluid came out of the disk, the wall shear stress went rapidly to zero. The laminar Stokes model of fluid flow is therefore valid for radii larger than r_{inlet} and smaller than r_{disk}. After a given duration of the flow, the disk was carefully removed, and the plate was transferred in a flat cuvette for microscopic examination of the remaining cell distribution. All experiments were performed at 21°C ± 1°C.

Data acquisition

The cell distribution remaining after an experiment was examined at low magnification (2.5×) under dark field illumination in a ICM405 inverted microscope (Zeiss, Le Pecq, France). A set of overlapping digital photographs was recorded (SP-Eye, Photonic Science, Millham, East Sussex, U.K.), extending from the origin of the flow to 15 mm in two orthogonal directions. The full picture was then reconstructed numerically using the Image Pro Plus software (Media Cybernetics, Silver Spring, MD). Spatial calibration of the setup was achieved using a Malassez cell. Additional pictures were also taken at 20 mm and at a distance greater than 40 mm (outside of the disk) from the origin of the flow. When visible, the origin of the flow was detected by the presence of the stagnation point, a zone of low local stress where some cells were remaining. Otherwise, the origin of the flow was determined as the symmetry point of the cell distribution along the orthogonal axis. Both methods allowed determination of the position of the center of the flow with a lateral precision better than 0.1 mm. The number of cells was then analyzed as a function of the distance to the center of the flow (Fig. 3 *B*), using the Image Pro Plus software. This analysis was performed along two orthogonal axes, in opposite directions with respect to the disk center. The cell density was then sampled using rectangular counting areas (0.6 × 1.5 mm) placed side by side along the axis (Fig. 3 *A*). Each area initially contained about 300 cells. No noticeable difference between the obtained distributions in each direction was observed, showing that the flow generated between the disk and the glass plate had the expected radial symmetry.

Data analysis

In most of the experiments reported here, the flow rate was selected so that the cell density on the plate after 5-min exposure to flow varied appreciably

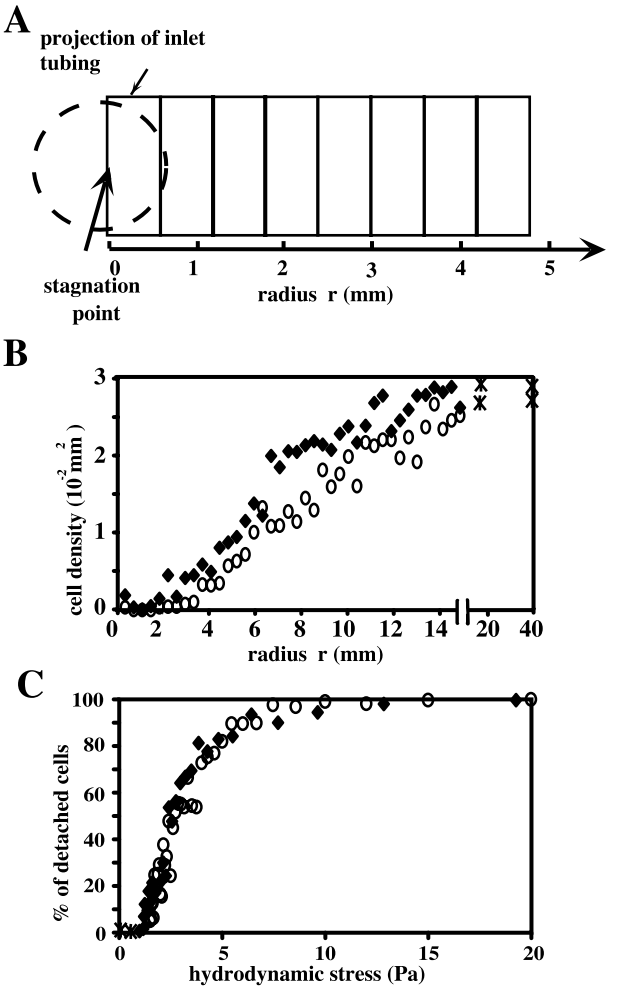

FIGURE 3 Data acquisition and analysis. (*A*) The remaining cell distribution is recorded by counting cells in rectangular areas. (*B*) Number of remaining cells versus distance r from the center of the flow, for $D = 36$ mL·min^{-1} (◆) and $D = 44$ mL·min^{-1} (○). (*C*) The detachment curve is obtained by plotting the percentage of detached cells versus the applied stress. This master curve is obtained by applying the relation $\sigma(r) = 3D\eta/\pi r e^2$, with $e = 0.21$ mm. The reference density ∗ is obtained at $r = 20$ mm and $r = 40$ mm (outside the disk).

over the first 15 mm from the center of the disk. The percentage of detached cells was obtained by normalization of the detached-cell density to the cell density on the plate recorded outside the disk ($r > 40$ mm), determined on three 1.5 × 2.2 mm counting areas (about 1000 cells). This density corresponded to the initial cell density separately determined, indicating that cells that were removed from the plate did not go to stick elsewhere in the measuring zone. This was confirmed by direct observation: cells were deposed in a circular 5-mm-diameter drop around the center of the plate and a detachment experiment conducted at $D = 50$ mL·min^{-1}. As expected from Fig. 3 *B*, all cells were detached, and these cells were found outside the 40-mm disk. Moreover, the detached cells were viable and still able to adhere to glass, as shown by the following control experiment: ~10^5 cells were detached by the radial flow and collected in the lower reservoir. The cells were pelleted, resuspended in Sörensen buffer, counted, and spread on another glass plate. After 10 min, the number of adherent cells was counted. More than 90% of the cells were able to bind tightly to the glass surface. The percentage of detached cells was then redrawn as a function of the wall shear stress calculated using Eq.

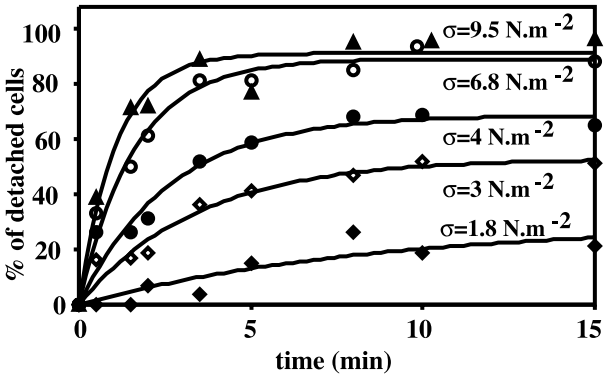

FIGURE 4 Cell detachment kinetics for different values of applied stress. The percentage of detached cells at the indicated shear stress as a function of time, are fitted with first-order kinetics: $n(t, \sigma) = e(\sigma)(1 - \exp(-k(\sigma)t))$. The uncertaincy is of statistical origin ($\sqrt{N}$). These curves are obtained for untreated cells on glass plates.

1 (Fig. 3 *C*). The validity of Eq. 1 was tested by comparing the detachment curves of Ax-2 cells on glass for different flow rates ($D = 36$, $D = 44$, $D = 56$ mL·min^{-1} not shown) or for different distances between the disk and the plate ($e = 0.21 \pm 0.01$, $e = 0.56 \pm 0.04$ mm, not shown). As shown in Fig. 3 *C*, a master curve is obtained when these data are plotted using Eq. 1, despite variations in the extent of the depletion zone (Fig. 3 *B*).

The cell-projected areas were acquired at higher magnification (10×) under dark field illumination. Cell-projected area was quantified using the Image Pro Plus Software. Cells touching the counting area were excluded from statistics.

Detachment kinetics

To study detachment kinetics, several experiments were performed, varying the duration of exposure to the shear flow from 30 s up to 15 min for glass plates, and from 5 min up to 60 min for DDS and APS. A set of detachment curves was obtained, using the preceding procedure. The percentage of detached cells was plotted as a function of time for regularly spaced values of the shear stress. A new set of curves was then drawn for these values of σ, representing the percentage of detached cells as a function of time (Fig. 4). Each of these curves was described by a first-order kinetics equation.

RESULTS

Cell detachment under shear flow obeys first-order kinetics

A set of experiments was carried out to study the effect of duration of a constant-applied shear stress on cell detachment. As show on Fig. 4, the percentage of detached cells increases with time and attains a plateau. The characteristic time to reach the plateau is shorter at higher stresses. The level of the plateau is higher for higher stresses. The kinetics are accurately described by a first-order relationship. In this way, the number of detached cells as a function of time t and shear stress σ, $n(\sigma, t)$, verifies

$$\frac{dn}{dt} = -kn, \tag{2}$$

confirming that cells detach independently. Moreover this indicates that the probability per unit time that a cell detaches is independent of time, excluding fatigue effect in the cell-detachment process. Solving Eq. 2 leads to

$$n(\sigma, t) = e(\sigma)[1 - \exp(-k(\sigma)t)], \tag{3}$$

where the values of both the detachment efficiency $e(\sigma)$ at infinite time and the detachment rate constant $k(\sigma)$ depend on the applied shear stress.

The detachment efficiency $e(\sigma)$

The detachment efficiency $e(\sigma)$ shown in Fig. 5 *A* exhibits a threshold behavior: below $\sigma_C = 0.9$ Pa, negligible detachment occurs, less than 10%. Above this value of the stress, the detachment efficiency increases rapidly with increasing stress, and, above 5 Pa, more than 90% of the cells have

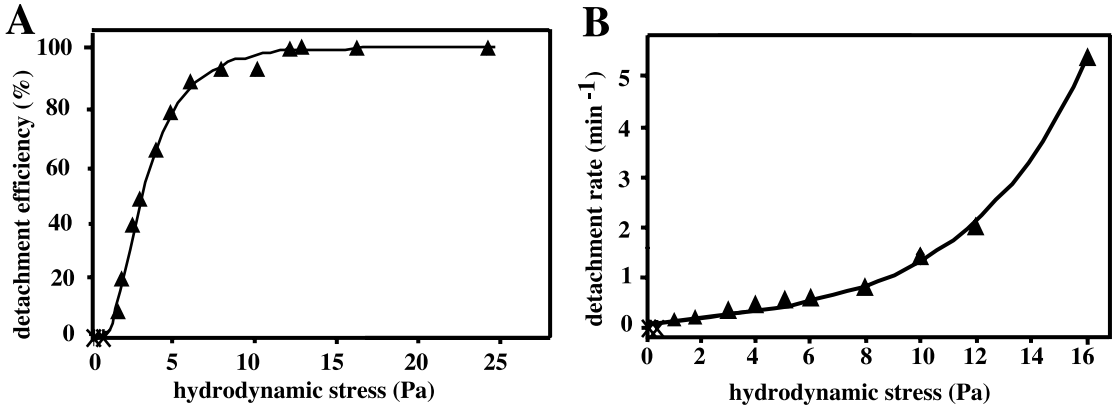

FIGURE 5 *Dictyostelium discoideum* detachment from glass. (*A*) Cell detachment efficiency $e(\sigma)$. (*B*) Cell detachment rate $k(\sigma)$. Curves are fitted with $e(\sigma) = \frac{1}{2}[1 - \mathrm{Erf}(\ln(\sigma/\sigma_{1/2})\sqrt{2}\tilde{\sigma})]$ and $k(\sigma) = k_0\exp\{(\sigma/4\sigma_0)^{1/2}\}/(\sigma/4\sigma_0)^{1/4}$. The best fit is obtained with $\sigma_{1/2} = 2.4$ Pa, $\tilde{\sigma} = 0.61$, $\sigma_0 = 7.3.10^{-2}$ Pa, and $k_0 = 0.11$ min^{-1}. Error bars are of the size of the symbols.

been detached in the end. A natural hypothesis is to assume that, for a given cell on a given surface, detachment will not happen below a threshold stress σ_t, whereas above this threshold, detachment will occur. If $f(\sigma_t)$ is the distribution function of threshold stresses in the cell population, $e(\sigma)$ is given by

$$e(\sigma) = \int_0^{\sigma} f(\sigma_t)\, d\sigma_t. \quad (4)$$

An accurate description of $f(\sigma_t)$ is obtained assuming a log-normal distribution of σ_t,

$$f(\sigma_t) = \frac{1}{\sqrt{2\pi}\,\tilde{\sigma}\sigma_t} \exp\left[-\frac{\ln^2(\sigma_t/\sigma_{1/2})}{2\tilde{\sigma}^2}\right], \quad (5)$$

where the two parameters $\sigma_{1/2}$, the stress at which detachment is most likely to occur, and $\tilde{\sigma}$, the nondimensional variance, are equal to 2.6 Pa and 0.6, respectively, for a glass plate. An explicit calculation of detachment efficiency (Eq. 4) leads to

$$e(\sigma) = \frac{1}{2}\left[1 - \mathrm{Erf}\left(\frac{\ln(\sigma/\sigma_{1/2})}{\sqrt{2}\,\tilde{\sigma}}\right)\right], \quad (6)$$

where Erf is the error function. Consequently, $\sigma_{1/2}$ corresponds to the stress required to detach 50% of adherent cells.

Correlation between threshold stress σ_t and cell-projected area

A clue about the mechanical parameter controlling the variability of threshold stress in cell detachment was obtained by examining the cell-projected areas S of the cells remaining on the plate after application of the flow. The observation of the remaining cells at a given position shows clearly that their average projected area is significantly lower (Student's test). For instance, at $\sigma = 4$ Pa, the average projected area of the remaining cells is $\bar{S} = 95 \pm 28\ \mu m^2$ to be compared with $\bar{S} = 110 \pm 20\ \mu m^2$ for $\sigma = 1$ Pa. It is therefore natural to correlate the threshold distribution function to the cell projected area distribution. Experimentally, the projected area distribution follows also a log-normal distribution

$$\rho(S) = \frac{1}{\sqrt{2\pi}\,\tilde{S}S} \exp\left[-\frac{\ln^2(S/S_{1/2})}{2\tilde{S}^2}\right], \quad (7)$$

with $S_{1/2} = 100\ \mu m^2$ and variance $\tilde{S}$ (see Fig. 6 *A*). Because both S and σ_t are distributed over the cell population as

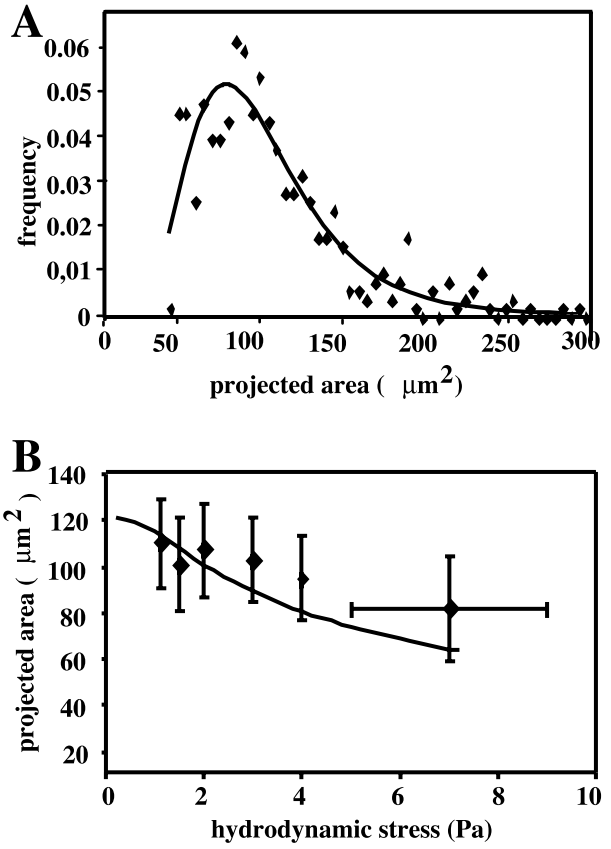

FIGURE 6 The threshold stress of cell detachment correlates with cell projected area. (*A*) Cell projected area distribution (glass plate) is a log-normal distribution: $\rho(S) = (\sqrt{2\pi}\tilde{S}S)^{-1}\exp(-\ln^2(S/S_{1/2})/2\tilde{S}^2)$ with $S_{1/2} = 100\ \mu m^2$ and $\tilde{S} = 0.67$. (*B*) Mean projected area of remaining cells after a detachment experiment as a function of hydrodynamic stress. The fit is derived from the cell-projected-area distribution and the postulated relation between threshold stress and area: $S = 1/\sigma_t^n$ (see Appendix).

log-normal distributions, a decreasing scaling relation was therefore searched between S and σ_t of the form,

$$\sigma_t = \frac{1}{S^n}. \quad (8)$$

It can indeed be shown that log-normal distributions are conserved by such transformations (Appendix). The threshold stress distribution was thus fitted using the projected cell area distribution and the former power law, leading to the value for the exponent $n = 1.6 \pm 0.2$. Finally, the mean remaining cell-projected area was calculated (see Appendix), as a function of the applied shear stress. As shown in Fig. 6 *B*, this expression fits experimental data, with no adjustable parameter, showing the consistency of this analysis.

The detachment rate constant $k(\sigma)$

The detachment rate constant $k(\sigma)$ characterizes the detachment kinetics at a given applied shear stress σ. It is the

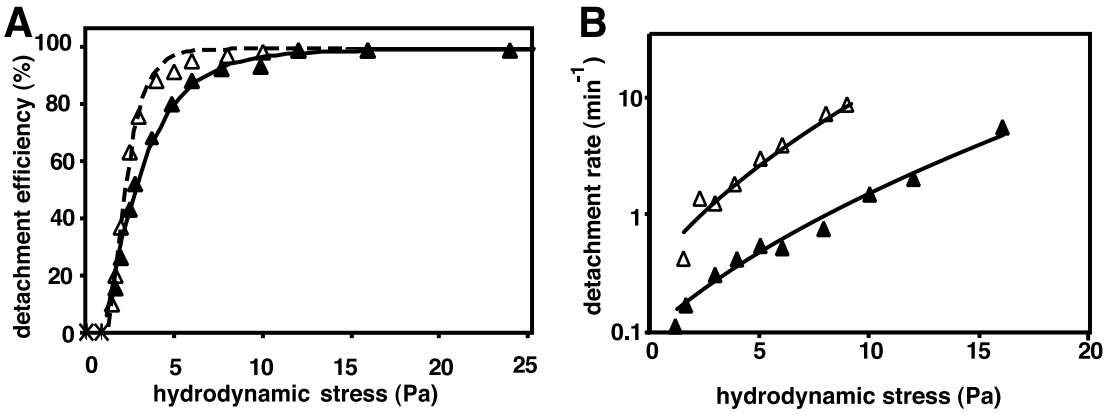

FIGURE 7 Effect of cytoskeleton depolymerization. ▲, Control cells; △, CIPC-treated cells, on glass plates. (*A*) Detachment efficiency $e(\sigma)$ fitted with Eq. 6. (*B*) Detachment rate $k(\sigma)$ fitted with Eq. 9. Values of the parameters are in Table 1.

inverse of the average time needed to detach a cell submitted to a given hydrodynamic stress. Figure 5 *B* shows that the detachment rate constant $k(\sigma)$ increases as the hydrodynamic stress increases. For high stress values, $k(\sigma)$ increases exponentially with σ, whereas, for small applied stresses, the detachment rate goes to zero as σ goes to σ_C. For high values of stress, the experimental curve is well fitted with the following expression, whose justification will be presented in (D. Garrivier, E. Decave, Y. Brechet, F. Bruckert, B. Fourcade, submitted for publication)

$$k(\sigma) = k_0 \frac{\exp(\sqrt{\sigma/4\sigma_0})}{(\sigma/4\sigma_0)^{1/4}}. \quad (9)$$

Two experimental parameters were determined: the intrinsic detachment rate k_0, which scales the detachment rate for given experimental conditions, and σ_0, the stress that scales the effect of the applied stress on the detachment rate. Data represented on Fig. 5 give $k_0 = 1.2.10^{-2}$ min^{-1} and $\sigma_0 = 8.10^{-2}$ Pa for a glass substrate. It should be noted that, contrary to the detachment efficiency, the detachment kinetics does not depend on the individual threshold of the cell. This point will be explained later.

Effect of cytoskeleton depolymerization

A cytoskeleton depolymerization agent, CIPC, was used to discriminate the role of the membrane and the cytoskeleton in the mechanism of cell detachment under shear flow. Previous studies on mammalian cells (Oliver et al., 1978) and on *Dictyostelium* (Aubry, 1994) have shown that CIPC induces a complete depolymerization of the actin and microtubule cytoskeleton. In the presence of the drug, cells take a symmetrical shape, as checked by microscopic examination (see Fig. 1). The detachment efficiency for CIPC-treated cells was very similar to the one for control cells (Fig. 7 *A* and Table 1). Both $\sigma_{1/2}$ and $\tilde{\sigma}$ depend, therefore, very weakly on cytoskeleton depolymerization. Projected area distributions were measured for both control cells and CIPC-treated cells and were found to be very similar. Consequently, identical values were found for the parameter n, which determines the analytical relation between cell projected area and threshold stress: $n = 1.6 \pm 0.2$.

In contrast, CIPC-treatment induced a dramatic increase in the detachment rate constant. Nevertheless, the qualita-

TABLE 1 Detachment parameters for *Dictyostelium discoideum* cells from various substrates in the presence or absence of CIPC

	Control Cells			CIPC-Treated Cells		
	Glass	DDS	APS	Glass	DDS	APS
k_0 (min^{-1})	$1.2.10^{-2} \pm 10^{-4}$	$1.1.10^{-4} \pm 5.10^{-5}$	—	0.11 ± 10^{-2}	$8.10^{-4} \pm 10^{-5}$	$7.10^{-5} \pm 2.10^{-5}$
σ_0 (Pa)	$8.0.10^{-2} \pm 10^{-2}$	$7.0.10^{-2} \pm 10^{-2}$	—	$8.25.10^{-2} \pm 10^{-2}$	$6.25.10^{-2} \pm 10^{-2}$	$8.75.10^{-2} \pm 10^{-2}$
$\sigma_{1/2}$ (Pa)	2.6 ± 0.1	7.7 ± 0.3	11.4 ± 0.2	2.4 ± 0.1	8.4 ± 0.3	11.80 ± 0.2
$\tilde{\sigma}$	0.64 ± 0.15	0.60 ± 0.17	0.69 ± 0.19	0.55 ± 0.12	0.61 ± 0.15	0.68 ± 0.15
$S_{1/2}$ (μm^2)	100 ± 10	155 ± 10	160 ± 10	105 ± 10	n.d.	n.d.
$\tilde{S}$	0.40 ± 0.06	0.32 ± 0.06	0.45 ± 0.06	0.33 ± 0.06	n.d.	n.d.
n	1.61 ± 0.2	1.85 ± 0.2	1.42 ± 0.2	1.66 ± 0.2	n.d.	n.d.

The parameters were obtained by fitting data presented of Fig. 5, 7, and 8 with Eqs. 6 and 9. Cell-projected areas were determined as described in Experimental Methods.
n.d., not determined.

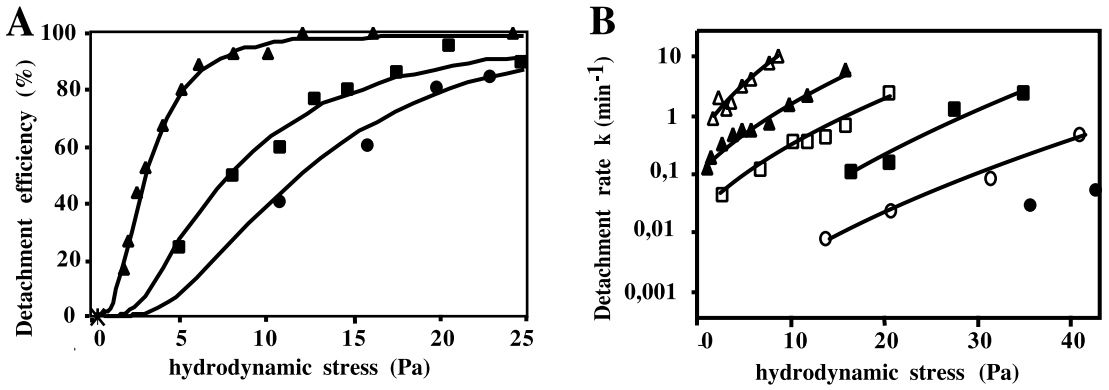

FIGURE 8 Effect of surface-treatment of the substrate. ▲, △, glass plates; ■, □, DDS-treated plates; ●, ○, APS-treated plates; *closed symbols*, control cells; *empty symbols*, CIPC-treated cells. (*A*) Detachment efficiency, fitted with Eq. 6. (*B*) Detachment rate fitted with Eq. 9. Values of the parameters are in Table 1.

tive properties of detachment kinetics were unchanged, with the two regimes described before (Fig. 7 *B*), the exponential ($\approx e^{\sqrt{\sigma}}$) domain at high stresses, and the decrease to zero as the stress goes down to 0.9 Pa. Fitting the data with Eq. 9 showed that σ_0 was not modified by CIPC-treatment, whereas k_0 was increased by a factor of 10. It can be concluded that the intrinsic detachment rate k_0 strongly depends on the cytoskeleton integrity.

Because CIPC is known to disrupt both the actin and tubulin networks, cells were also treated with nocodazole, a microtubule depolymerization agent. No difference was observed in the detachment curves of CIPC-, nocodazole-treated, or control cells after applying the flow for 10 min (apparent $\sigma_{1/2} = 2.7$, 2.6, or 2.4 Pa, respectively). In contrast, applying the flow for 30 s resulted in a clear difference between CIPC-treated cells' distribution compared to that of nocodazole-treated or control cells (apparent $\sigma_{1/2} = 6.6$, 10.3, or 12.3 Pa, respectively). The lower value of the apparent $\sigma_{1/2}$ for CIPC-treated cells after 30 s indicates that the kinetics of cell detachment is faster. The increase for detachment kinetics of CIPC-treated cells is thus due to actin microfilament depolymerization, because nocodazole affects only microtubules.

Modifying cell–substrate interaction by surface treatment

To modify cell–substrate interaction, detachment experiments were performed using two additional different substrates obtained by covalent coupling of silane derivatives to glass, DDS and APS. Detachment efficiency exhibits the same qualitative behavior for the three substrates (Fig. 8 *A*): existence of a critical stress under which no cell is detached, and a domain of sharp increase in the percentage of detached cells up to 100%. The detachment curves are fitted with Eq. 6, resulting in: $\sigma_{1/2}^{\text{glass}} = 2.6$ Pa, $\sigma_{1/2}^{\text{DDS}} = 7.7$ Pa, and $\sigma_{1/2}^{\text{APS}} = 11.40$ Pa (see Table 1). Consequently, these three substrates can be ranged as glass $<$ DDS $<$ APS in order of increasing adhesiveness. Note that the variance of threshold stress distribution function $\tilde{\sigma}$ is constant for all materials. From the projected cell area distribution and the threshold stress distribution are derived values for n, the parameter characterizing the relation between S and σ_t. Because $\tilde{S}$ and $\tilde{\sigma}$ do not vary, n is also found to be constant whatever the substrate: $n = 1.6 \pm 0.2$.

Figure 8 *A* shows the changes in detachment rate consecutive to the changes in substrate. Results for the three substrates are given, both for control cells and for CIPC-treated cells. Only the high stress part of the curves with DDS- and APS-treated plates were attainable, because the kinetics of detachment for those substrates were so low at lower stresses that the experimental time window would have to be extended beyond one hour. The same reason impeded the quantitative study of the detachment rate for control cells on APS-treated plates. Detachment rate curves are fitted with Eq. 9. This shows (Table 1) that σ_0 is roughly constant for all materials, whereas k_0 is the most sensitive parameter changing by four orders of magnitude from glass to APS (Table 1). In summary, two major effects are found by changing the cell–substrate interaction: a change in $\sigma_{1/2}$ measuring the strength of adhesiveness, and an opposite change in k_0.

Relation between detachment efficiency and kinetics

As a conclusion of this experimental part, three experimental parameters are determined: $\sigma_{1/2}$, k_0, σ_0. They deal with the statics and kinetics of cell detachment on solid substrates. The first two quantities however do not vary independently. As shown in Fig. 9, k_0 decreases by more than three orders of magnitude as $\sigma_{1/2}$ increases tenfold. For

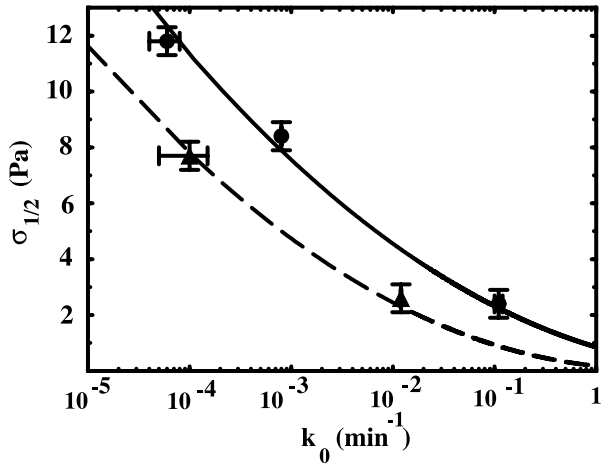

FIGURE 9 Relationship between $\sigma_{1/2}$, the stress detaching 50% of the cells, and k_0, the intrinsic detachment rate. ▲, Control cells; ●, CIPC-treated cells. These curves were fitted with Eq. 10, resulting in $\tilde{k} = 3.0$ min^{-1} for control cells and $\tilde{k} = 26.0$ min^{-1} for CIPC-treated cells.

rationale explained in the discussion, the following relationship was used to fit these data.

$$k_0 = \tilde{k} \exp\left[-\left\{ \frac{\sigma_{1/2}}{\sigma_0} - \left(\frac{\pi^2}{3} - 2 \right) \right\}^{1/2} \right], \qquad (10)$$

where $\sigma_{1/2}$ is scaled by $\sigma_0 = 8.10^{-2}$ Pa fixed at the value determined from the kinetics. A good fit of the data was obtained with a single adjustable parameter $\tilde{k}$, having the dimension of a detachment rate. For control and CIPC-treated cells, $\tilde{k} = 3.0$ and $\tilde{k} = 26.0$ min^{-1}, respectively (see Fig. 9). In this relation, the prefactor $\tilde{k}$ bears all the effect of the cytoskeleton, whereas the exponential term depends only on the substrate material through $\sigma_{1/2}$.

DISCUSSION

Evidence for a peeling model of cell detachment

This experimental study shows that cell detachment depends on three parameters: $\sigma_{1/2}$, the hydrodynamic stress needed to detach 50% of the cells at steady state; $\tilde{k}$, the detachment rate scaling factor; and σ_0, which scales both the increase of $k(\sigma)$ with σ and the increase of k_0 with $\sigma_{1/2}$ (see Eq. 9 and 10). The first parameter, $\sigma_{1/2}$, is characteristic of the cell–substrate interaction and is insensitive to actin microfilament depolymerization. In this work, the strength of cell–substrate interaction was modulated by changing the chemical properties of the glass surface. Previous studies showed that $\sigma_{1/2}$ is also sensitive to the nature of the fluid bathing the cells (nutritive medium versus phosphate buffer), which may decrease adhesion because some surface receptors such as lectins are saturated, and to the presence of the Phg1 adhesion protein (Cornillon et al., 2000). The second parameter, $\tilde{k}$, is characteristic of the mechanical properties of the cell, because it is insensitive to the substrate chemistry, but increases by a factor of 10 upon actin depolymerization. The actual kinetics of cell detachment on a given substrate results from both $\tilde{k}$ and $\sigma_{1/2}$. The third parameter, σ_0, is a reference stress, constant under our experimental conditions.

Our work confirms the existence of a threshold stress required to detach cells adhering on flat surfaces. A comparable behavior of cells under external constraint was previously reported by Truskey and Proulx (1993), Thoumine et al. (1996), DiMilla et al. (1991), and Goldstein and DiMilla (1997), who applied similar hydrodynamic forces or tangential centrifugal forces. Contrary to previous reports, where a static representation of cell adhesion was used to interpret the threshold, we show here that the threshold value is closely related to the detachment kinetics (Fig. 9 and Eq. 10). The threshold stress should therefore be interpreted in the frame of a dynamical model of cell detachment, and does not result from a simple static balance of forces in the cell at rest. In this frame, cell detachment corresponds to a transition between two regimes.

Below the threshold stress, cells respond to the external forces by changing the contact angle of the plasma membrane with the substrate. This has been directly observed for *D. discoideum* cells adhering on glass and submitted to a stress of about 0.1 Pa (Simson et al., 1998). It is possible that, under these conditions, a very slow rolling motion of the cells occurs, but this has not yet been reported in this experimental system. The position and number of filopodia was also apparently not affected under these subthreshold conditions (Simson et al., 1998). Under these conditions, cell adhesion is in a stable equilibrium situation.

Above the threshold stress, the cells detach from the surface and are dragged away outside of the chamber by the flow. This is quite visible when the applied flow is high enough to detach significant amounts of cells. Cells are still alive and able to adhere back to a glass surface when used in another experiment. What happens to the cell when the external stress reaches the threshold value? One possibility could be that the cell internal structure suddenly collapses when the applied forces reach a critical value. The collapse would convert the flat cell–substrate interface into a more spherical shape, severely reducing the contact zone. It was indeed shown that fibroblasts submitted to lateral centrifugation forces elongate before detaching from the substrate (Rees et al., 1977; Thoumine et al., 1996). In this case, part of the mechanical work associated with cell detachment would consist of cell deformation, dragging the nucleus through the viscous cytoplasm. However, although we do not dismiss that some deformation of the cell precedes its detachment, it seems unlikely that adhesive bonds break simultaneously. If the cell structure was collapsing at threshold, the threshold value would indeed depend on the presence of the cytoskeleton, which we have shown not to be the case. The simplest interpretation is that the adhesive

bonds break progressively with time, starting at the edge of the cell facing the flow. This process will create a pathway of low activation energy, leading to cell detachment. The threshold barrier is envisioned as the force above which cells are no more able to adapt the contact area to the additional membrane tension induced by the flow drag. Above the threshold, the forces become sufficient to break irreversibly the adhesive bridges. The kinetics of cell detachment would therefore correspond to the propagation velocity of a fracture between the cell and the substrate. Below the threshold, spontaneous reformation of the bonds would oppose this "unzipping" effect.

The breaking of the equilibrium situation, where the density of bonds adapts to the external forces so that the rate of bond reformation equilibrates that of bond dissociation, explains the quasi-exponential increase of the cell-detachment rate with the applied stress. Application of Kramers' theory to the case receptor–ligand interaction under constraint predicts that the dissociation rate of a bond indeed increases exponentially with the applied force (Bell, 1978). This relationship has been verified in a variety of experimental situations, including the case of adhesion receptors (Bongrand, 1999). Conversely, it is expected that reassociation rate decreases as the distance between the membrane and the substrate increases, a geometrical factor favored by the forces leading to detachment. When the stress passes its threshold value, the dissociation rate of the bonds rapidly overcomes the association rate. The rapidly varying cell detachment kinetics are therefore well explained by a peeling model.

Quantitative considerations on $\sigma_{1/2}$ also support the view that detachment occurs by a peeling process. First, the total cell–substrate energy is much higher than the mechanical work hydrodynamic forces perform to detach the cell. The former was estimated for *D. discoideum* cells adhering on glass by the contact angle between the plasma membrane and the flat substrate (Simson et al., 1998). The total adhesion energy of the cell at rest is $W_{adh}S_{cont}$, where $W_{adh} \approx 22.10^{-6}$ J/m^2 (Simson et al., 1998) and $S_{cont} \approx 120\ \mu$m^2 are the cell–substrate surface adhesion energy and contact area, respectively. *Dictyostelium* cells detach from glass at an average hydrodynamic stress $\sigma_{1/2} = 2.6$ Pa. Approximating the cell by a solid hemispheric cup of contact area S_{cont} gives an upper limit for the force exerted on the cell as the result of viscous drag: $F = \sigma_{1/2}S_{cont} \approx 300$ pN. This force is small, within the range of forces exerted to break single noncovalent molecular complexes (Baumgartner et al., 2000; Carl et al., 2001). The work done by this force during a hypothetical simultaneous disruption of all cell bonds, in an ideal quasistatic process, scales as $F\delta_{off} = \sigma_{1/2}S_{cont}\delta_{off}$, where δ_{off} is the range of the bond, typically 1 Å. The ratio between the two energies is $W_{adh}/(\sigma_{1/2}\delta_{off}) \approx 10^5$. The energy dissipated by the hydrodynamic flow in breaking molecular bonds is therefore 10^5 times less than the total cell–substrate interaction energy. Simultaneous breaking of all molecular bonds is therefore not possible. We propose to define as adhesive bridge the individual adhesive unit able to be broken by hydrodynamic forces. This may encompass one or several adhesion proteins. From the above order of magnitude estimates, we can suggest that cell–substrate adhesion at rest is made of 10^5 of such bridges, each contributing 2.10^{-20} J $\approx 5\ k_BT$.

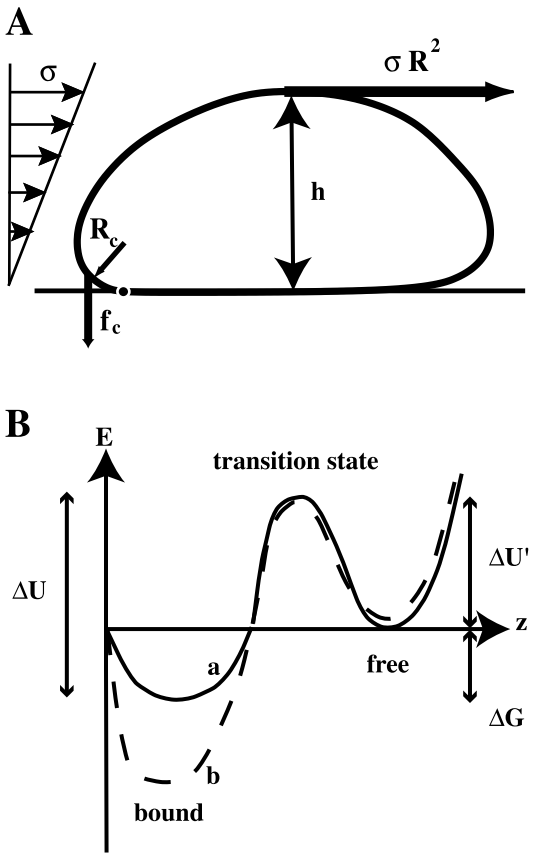

FIGURE 10 (*A*) Model used to describe the adhesive zone near the contact line. The hydrodynamic shear rate is concentrated on the top part of the cell of size R and gives a total force that scales as σR^2. At equilibrium, the moment of hydrodynamic forces with respect to the contact line is balanced with the moment of the restoring forces exerted by the adhesive bridges on the cell margin. The lever arm of the hydrodynamic forces is h, scaling as R, and the one of the restoring force is R_c. (*B*) Energy landscape for an unstretched adhesive bridge. (*a*) Reference situation, a transition state separates the bound and free states of the adhesive bridge. (*b*) Changing the substrate modifies the energy of the bound state.

A second line of evidence arguing in favor of a peeling process comes from the size dependence of the individual cell threshold. As already mentioned, cells with a large projected area detach more easily from the substrate. The scaling relation $\sigma_t \approx 1/S^n$ indeed links the threshold stress σ_t to the cell projected area S. Assuming $S \approx R^2$, where R is the typical size of the cell, the threshold stress then scales as $\sigma_t = 1/R^{2n}$. An increase in cell size indeed has two opposite effects. On the one hand, the total cell–substrate interaction energy is expected to increase with cell contact area, as is

the number of adhesion proteins per cell. On the other hand, the total drag forces of the fluid on the cell also increase (see Truskey and Proulx (1993) for details about the force and torque acting on a solid cell of various shape). If the effect of the hydrodynamic forces was to detach all adhesion proteins at the same time, no effect of size would be expected, because both hydrodynamic forces and adhesion energy scale in the same way with S_{cont}. In contrast, in a peeling model, the forces concentrate at the edge of the cell. Assuming that cells have typical size R (see Fig. 10 *A*), the force due to the hydrodynamic drag scales as σR^2 and the equivalent mechanical moment with respect to the contact line scales as $\sigma R^2 h$. Assuming $h \approx R$, the mechanical moment with respect to the contact line thus scales as σR^3. At threshold, this moment equals the total restoring moment, which results from the stretching of the connected adhesive bridges in the adhesive belt. This moment scales as $f_c R_c$, where f_c is the critical force applied on the adhesive bridge, which is peeled first, and R_c is the radius of curvature of the membrane in the adhesive belt (see Fig. 10 *A* and Simson et al. (1998)). Assuming that R_c is independent of cell size, the hydrodynamic stress scales with the cell radius as $\sigma_t \propto 1/R^3 \approx 1/S^{3/2}$. Experimental data support this picture, because the exponent n ranges from 1.4 to 1.8, depending on substrate treatment.

Microscopic interpretation of the cell detachment kinetics

The peeling model introduced in D. Garrivier, E. Decave, Y. Brechet, F. Bruckert, B. Fourcade, (submitted for publication) describes the passive behavior of the margin of cells attached by discrete adhesive bridges to the substrate surface under hydrodynamic stress. Three supplementary hypotheses of the model are that the cells are locally deformable, that the density of adhesion proteins in the contact area is higher than elsewhere in the plasma membrane, and that the microscopic detachment rate of adhesive bridges on solid surfaces depends on the local applied force following Kramers theory (see Fig. 10 *B*). The homogeneity in adhesion-protein density may originate from lateral diffusion in the plasma membrane. This model shows the existence of a threshold between two adhesion regimes. For a given cell, below the threshold stress σ_t, the "adhesive belt" near the edge of the cell facing the flow resists the stress, adapting the distribution of adhesive bridges by stretching bound adhesion proteins in the contact region between the cell and the substrate. In this way, elastic energy is stored in the adhesive belt. The limit to this mechanism comes from the spontaneous rupture of the adhesive bridges under the elastic forces (a thermally-activated process). At a critical force, corresponding to the experimental threshold stress σ_t, adhesive bridges are no more able to store elastic energy, and the cell margin starts moving. Because the stress at the cell margin varies with the cell radius R as $1/R^3$, the size distribution of the cells translates into a threshold stress distribution, with an average threshold stress close to $\sigma_{1/2}$. Above the threshold stress σ_t, a regime of fracture propagation at constant velocity v becomes possible. During this peeling process, the elastic energy stored in the adhesive bridges is dissipated, the dissociation rate of the adhesive bridges limiting the propagation speed of the fracture. This results in an apparent first-order rate of cell detachment $k = v/R$, where R is the typical cell size. The cell detachment rate is thus interpreted as the inverse of the time needed for the fracture to propagate under the cell. It is noteworthy that, because the fracture propagation velocity v is independent of the cell size, the detachment rate of the cells is almost independent of the individual threshold σ_t. This explains why, within experimental uncertainties, all cells that detach at a given stress follow the same kinetics, whatever their individual threshold (see Eq. 3). The detachment rate increases rapidly as a function of the applied stress, according to Eq. 9 (see D. Garrivier, E. Decave, Y. Brechet, F. Bruckert, B. Fourcade, submitted for publication). Near the threshold stress, a range where the cell-detachment rate increases linearly with the applied stress is also predicted, that would connect the $v = 0$ solution to the above regime, but this transition could not be observed with precision under our experimental conditions.

As a consequence of the microscopic nature of this model, it is possible to relate experimentally attainable parameters to microscopic parameters of interest. The intrinsic detachment rate k_0 is directly related to the dissociation rate of the adhesion proteins at the molecular level: $k_0 = k_{off}^0 \xi_0 / R\sqrt{2}$, ξ_0 being the size of the adhesive belt. σ_0 reflects the strain repartition across the adhesive belt and is therefore linked to the adhesion protein density n_0: $\sigma_0 = n_0 \Sigma$, where Σ is a constant. A remarkable result obtained in the theoretical part is that σ_t and σ_0 are linked, with their ratio being a function of only one parameter, i.e. K_e, the local equilibrium constant of the adhesive bridges (see D. Garrivier, E. Decave, Y. Brechet, F. Bruckert, B. Fourcade, (submitted for publication). Averaging on the individual thresholds, an analogous relation can be derived for $\sigma_{1/2}$. The ratio can alternatively be expressed as a function of ΔG, the adhesion energy per receptor. An explicit relation was obtained in the limiting case $K_e \gg 1$,

$$\frac{\sigma_{1/2}}{\sigma_0} = (\ln K_e)^2 + \pi^2/3 - 2 = (\Delta G / k_B T)^2 + \pi^2/3 - 2. \quad (11)$$

In the case of *D. discoideum* adhesion on glass, an interaction energy per adhesion protein $\Delta G \approx 5.5 k_B T$ can be estimated from $\sigma_{1/2} = 2.6$ Pa and $\sigma_0 = 8.10^{-2}$ Pa. In the case of DDS- or APS-treated glass, where σ_0 is similar, the adhesion energy rises to $10.4 k_B T$ and $12.5 k_B T$, respectively. This relation exemplifies the usefulness of measuring both static ($\sigma_{1/2}$) and kinetic (σ_0) parameters of cell detachment

to relate macroscopic parameters to molecular quantities (Zhu, 2000). In contrast, using the formula derived by Dembo et al. (1988) requires the knowledge of the density of adhesion molecules n_0 and the contact angle θ, as evidenced by the expression of the critical tension,

$$T_c = \frac{n_0 k_B T}{1 + \cos\theta} \ln(1 + K_e).$$

It should be stressed that studying the kinetics of cell detachment also ensures that steady state was attained for measuring $\sigma_{1/2}$. Deriving $\sigma_{1/2}$ from the remaining cell distribution on APS-treated glass after 15 min would indeed result in a serious overestimation of this parameter by a factor of 2–3. It should be also noted that, depending on the flow rate and the disk plate height e, the span of $\sigma_{1/2}$ that can be probed in such experiments (0.1 to 10 Pa, see Eq. 1) is well adapted to the range of most cell–substrate interactions. Hence the flow detachment assay mimics physiologically relevant situations.

The above Eq. 11 allows interpretation in simple terms of the experimental relationship between $\sigma_{1/2}$ and k_0 parameters, obtained for two cell populations on the same set of substrates. The variation of k_0 with $\sigma_{1/2}$ is due to changes in the microscopic dissociation rate constant k_{off}^0, describing the interaction of the adhesion proteins with the substrate,

$$k_0 = k_{off}^0 \frac{\xi_0}{R\sqrt{2}} = k_{on}^0 \frac{\xi_0}{R\sqrt{2}} K_e^{-1}$$

$$= \tilde{k} \exp\left[-\left\{ \frac{\sigma_{1/2}}{\sigma_0} - \left(\frac{\pi^2}{3} - 2 \right) \right\}^{1/2} \right].$$

The exponential factor in Eq. 10 corresponds, therefore, to the equilibrium constant K_e. The prefactor $\tilde{k} = k_{on}^0 \xi_0 / R\sqrt{2}$ is directly related to the microscopic association rate constant k_{on}^0. The simplest interpretation of the data obtained with the three substrates tested (glass, DDS, APS) is that the association rate constant k_{on}^0 is similar, whereas the dissociation rate constant k_{off}^0 increases (see Fig. 10 *B*). An underlying hypothesis is that the nature of the adhesive bridges is the same on the three substrates. This is likely, because σ_0, which is proportional to the number of adhesive bridges, is constant under these conditions.

It remains to directly show that detachment kinetics are controlled by the formation of a peeling front at the cell–substrate interface. Preliminary microscopic observation of the evolution of the contact area during flow confirms this interpretation of the detachment process (manuscript in preparation). As for the striking effect of cytoskeleton depolymerization on the kinetics of cell detachment, its influence can be possibly related to the details of cell motion mechanisms.

APPENDIX: LOG-NORMAL DISTRIBUTIONS

Description of log-normal distributions

Threshold stresses and cell-projected area are both log-normally distributed over the cell population, i.e., the threshold stress distribution function $f(\sigma_t)$ and the cell projected-area distribution $\rho(S)$ are both of the form

$$f(x) = \frac{1}{\sqrt{2\pi}\tilde{x}x} \exp\left(-\frac{\ln^2(x/x_{1/2})}{2\tilde{x}^2} \right), \qquad \text{(A1)}$$

where $\tilde{x}$ is the variance of the distribution.

Power-law transformation

The following decreasing power law has been postulated between S and $\sigma_{1/2}$: $S = 1/\sigma_t^n$. Thus $f(\sigma_t)$ is obtained by $f(\sigma_t)d\sigma_t = \rho(S)dS$. One has

$$\left| \frac{dS}{d\sigma_t} \right| = \frac{n}{\sigma_t^{n+1}}.$$

Hence,

$$f(\sigma_t) = \rho(S(\sigma_t)) \frac{dS}{d\sigma_t}$$

$$= \frac{1}{\sqrt{2\pi}(\tilde{S}/n)\sigma_t} \exp\left(-\frac{\ln^2(\sigma_{1/2}/\sigma_t)}{2(\tilde{S}/n)^2} \right) \qquad \text{(A2)}$$

$$= \frac{1}{\sqrt{2\pi}\tilde{\sigma}\sigma_t} \exp\left(-\frac{\ln^2(\sigma_t/\sigma_{1/2})}{2\tilde{\sigma}^2} \right), \qquad \text{(A3)}$$

with $\tilde{\sigma} = \tilde{S}/n$. Thus, lognormal distributions are conserved in this transformation.

Calculation of mean cell-projected area of remaining cells after a detachment experiment as a function of σ

At a given value of applied stress σ, cells remaining have a threshold stress greater than σ, i.e., a cell-projected area less than $S(\sigma)$. Hence, the mean projected area of remaining cells after a detachment experiment is

$$\bar{S} = \frac{\int_0^{S(\sigma)} S\rho(S)\, dS}{\int_0^{S(\sigma)} \rho(S)\, dS}. \qquad \text{(A4)}$$

Finally,

$$\bar{S} = S_{1/2} \exp(n^2\tilde{\sigma}^2/2) \frac{1 - \mathrm{Erf}\left(\frac{n\tilde{\sigma}^2 - \ln(\sigma_{1/2}/\sigma)}{\sqrt{2}\tilde{\sigma}} \right)}{1 - \mathrm{Erf}\left(-\frac{\ln(\sigma_{1/2}/\sigma)}{\sqrt{2}\tilde{\sigma}} \right)}. \qquad \text{(A5)}$$

Grant sponsors: the Commissariat l'Energie Atomique, the Centre National de la Recherche Scientifique and the Université Joseph Fourier, Grenoble, France. This work was also supported by a grant "Adhésion Cellule-Matériau" from the Institut National de la Santé et de la Recherche Médicale and the CNRS-Matériaux. E.D. and D.G. were recipients of a MENRT and a CNRS fellowship respectively. We thank Bernard Sartor and Véronique Collin-Faure for excellent technical assistance.

REFERENCES

Albelda, S. M., and C. A. Buck. 1990. Integrins and other cell adhesion molecules. *FASEB J.* 4:2868–2880.

Ashworth, J. M., and D. J. Watts. 1970. Metabolism of the cellular slime mould *Dictyostelium discoideum* grown in axenic culture. *Biochem. J.* 119:175–182.

Aubry, L. 1994. Endocytose de phase fluide chez l'amibe *Dictyostelium discoideum*. Ph.D. thesis. Universite Joseph Fourier, Grenoble, France.

Baumgartner, W., P. Hinterdorfer, W. Ness, A. Raab, D. Vestweber, H. Schindler, and D. Drenckhahn. 2000. Cadherin interaction probed by atomic force microscopy. *Proc. Natl. Acad. Sci. U.S.A.* 97:4005–4010.

Bell, G. I. 1978. Models for the specific adhesion of cells to cells. *Science.* 200:618–627.

Bongrand, P. 1999. Ligand–receptor interactions. *Rep. Prog. Phys.* 62: 921–968.

Bongrand, P., C. Capo, and R. Depieds. 1982. Physics of cell adhesion. In Progress in Surface Science. Vol. 12. Pergamon Press Ltd., 217–286.

Bozzaro, S., and E. Ponte. 1995. Cell adhesion in the life cycle of *Dictyostelium. Experientia.* 51:1175–1188.

Cantat, I. 1999. Dynamique de vésicules en adhésion. Ph.D. thesis. Universite Joseph Fourier, Grenoble, France.

Carl, P., C. H. Kwok, G. Manderson, D. W. Speicher, and D. W. Discher. 2001. Forced unfolding modulated by disulfide bonds in the Ig domains of a cell adhesion molecule. *Proc. Natl. Acad. Sci. U.S.A.* 98:1565–1570.

Chan, P. Y., M. B. Lawrence, M. L. Justin, L. M. Ferguson, D. E. Golan, and T. A. Springer. 1991. Influence of receptor lateral mobility on adhesion strengthening between membranes containing LFA-3 and CD2. *J. Cell Biol.* 115:245–255.

Chia, C. P. 1996. A 130-kDa plasma membrane glycoprotein involved in *Dictyostelium* phagocytosis. *Exp. Cell Res.* 227:182–189.

Cornillon, S., E. Pech, M. Benghezal, K. Ravanel, E. Gaynor, F. Letourneur, F. Bruckert, and P. Cosson. 2000. Phg1p is a nine-transmembrane protein superfamily member involved in *Dictyostelium* adhesion and phagocytosis. *J. Biol. Chem.* 275:34287–34292.

Cozens-Roberts, C., J. A. Quinn, and D. A. Lauffenburger. 1990a. Receptor-mediated adhesion phenomena. I. Model studies with the radial-flow detachment assay. *Biophys. J.* 58:107–125.

Cozens-Roberts, C., J. A. Quinn, and D. A. Lauffenburger. 1990b. Receptor-mediated cell attachment and detachment kinetics. II. Experimental model studies with the radial-flow detachment assay. *Biophys. J.* 58: 857–872.

de Lozanne, A., and J. A. Spudich. 1987. Disruption of the *Dictyostelium* myosin heavy chain gene by homologous recombination. *Science.* 236: 1086–1091.

de Priester, W., P. Riegman, and A. Vonk. 1988. Effects of microtubule disrupting agents on chemotactic events in *Dictyostelium discoideum. Eur. J. Cell Biol.* 46:94–97.

Dembo, M., D. C. Torney, K. Saxman, and D. A. Hammer. 1988. The reaction-limited kinetics of membrane-to-surface adhesion and detachment. *Proc. R. Soc. (Lond.). B.* 234:55–83.

DiMilla, P. A., K. Barbee, and D. A. Lauffenburger. 1991. Mathematical model for the effects of adhesion and mechanics on cell migration speed. *Biophys. J.* 60:15–37.

DiMilla, P. A., J. A. Stone, J. A. Quinn, S. M. Albelda, and D. A. Lauffenburger. 1993. Maximal migration of human smooth muscle cells on fibronectin and type IV collagen occurs at an intermediate attachment strength. *J. Cell Biol.* 122:729–737.

Dunon, D., L. Piali, and B. A. Imhof. 1996. To stick or not to stick: the new leukocyte homing paradigm. *Curr. Opin. Cell Biol.* 8:714–723.

Evans, E., and A. Leung. 1984. Adhesivity and rigidity of erythrocyte membrane in relation to wheat germ agglutinin binding. *J. Cell Biol.* 98:1201–1208.

Goldman, A. J., R. G. Cox, and H. Brenner. 1967. Slow viscous motion of a sphere parallel to a plane wall-*II*-Couette flow. *Chem. Eng. Sci.* 22:653–660.

Goldstein, A. S., and P. A. DiMilla. 1997. Application of fluid mechanic and kinetic models to characterize mammalian cell detachment in a radial-flow chamber. *Biotechnol. Bioeng.* 55:616–629.

Hynes, R. O. 1987. Integrins: a family of cell-surface receptors. *Cell.* 48:549–554.

Kamath, K. R., M. J. Danilich, R. E. Marchant, and K. Park. 1996. Platelet interactions with plasma-polymerized ethylene oxide and *N*-vinyl-2-pyrrolidone films and linear poly(ethylenoxide) layer. *J. Biomater. Sci. Polymer Edn.* 7:977–988.

Kay, R. R., and J. G. Williams. 1999. The *Dictyostelium* genome project: an invitation to species hopping. *Trends Genet.* 15:294–297.

Manstein, D. J., H. P. Schuster, P. Morandini, and D. M. Hunt. 1995. Cloning vectors for the production of proteins in *Dictyostelium discoideum. Gene.* 162:129–134.

Morio, T., H. Urushihara, T. Saito, Y. Ugawa, H. Mizuno, M. Yoshida, R. Yoshino, B. N. Mitra, M. Pi, T. Sato, K. Takemoto, H. Yasukawa, J. Williams, M. Maeda, I. Takeuchi, H. Ochiai, and Y. Tanaka. 1998. The *Dictyostelium discoideum* developmental cDNA project: generation and analysis of expressed sequence tags from the first-finger stage of development. *DNA Res.* 5:335–340.

Oliver, J. M., J. A. Krawiec, and R. D. Berlin. 1978. A carbamate herbicide causes microtubule and microfilament disruption and nuclear fragmentation in fibroblasts. *Exp. Cell Res.* 116:229–237.

Palecek, S. P., J. C. Loftus, M. H. Ginsberg, D. A. Lauffenburger, and A. F. Horwitz. 1997. Integrin–ligand binding properties govern cell migration speed through cell–substratum adhesiveness. *Nature.* 385:537–539.

Pierres, A., A. M. Benoliel, and P. Bongrand. 1995. Measuring the lifetime of bonds made between surface-linked molecules. *J. Biol. Chem.* 270: 26586–26592.

Pierres, A., A. M. Benoliel, P. Bongrand, and P. A. Van Der Merwe. 1996. Determination of the lifetime and force dependence of interactions of single bonds between surface-attached CD2 and CD48 adhesion molecules. *Proc. Natl. Acad. Sci. U.S.A.* 93:15114–15118.

Pierres, A., O. Tissot, B. Malissen, and P. Bongrand. 1994. Dynamic adhesion of CD8-positive cells to antybody-coated surfaces: the initial step is independent of microfilaments and intracellular domains of cell-binding molecules. *J. Cell Biol.* 125:945–953.

Rees, D. A., C. W. Lloyd, and D. Thom. 1977. Control of grip and stick in cell adhesion through lateral relationships of membrane glycoproteins. *Nature.* 267:124–128.

Simson, R., E. Wallraff, J. Faix, J. Niewoehner, G. Gerisch, and E. Sackmann. 1998. Membrane bending modulus and adhesion energy of wild-type and mutant cells of *Dictyostelium* lacking talin or cortexillins. *Biophys. J.* 74:514–522.

Takeichi, M. 1990. Cadherins: a molecular family important in selective cell–cell adhesion. *Annu. Rev. Biochem.* 59:237–252.

Thoumine, O., A. Ott, and D. Louvard. 1996. Critical centrifugal forces induce adhesion rupture or structural reorganization in cultured cells. *Cell Motil. Cytoskel.* 33:276–287.

Truskey, G. A., and T. L. Proulx. 1993. Relationship between 3T3 cell spreading and the strength of adhesion on glass and silane surfaces. *Biomaterials.* 14:243–254.

Turner, D. C., C. Chang, K. Fang, S. L. Brandow, and B. M. Murphy. 1995. Selective adhesion of functional microtubules to patterned silane surfaces. *Biophys. J.* 69:2782–2789.

Vogel, G., L. Thilo, H. Schwarz, and R. Steinhart. 1980. Mechanism of phagocytosis in *Dictyostelium discoideum*: phogocytosis is mediated by different recognition sites as disclosed by mutants with altered phagocytotic properties. *J. Cell Biol.* 86:456–465.

Williams, K. L., R. H. Kessin, and P. C. Newell. 1974. Genetics of growth in axenic medium of the cellular slime mould *Dictyostelium discoideum. Biochem. J.* 247:142–143.

Zhu, C. 2000. Kinetics and mechanics of cell adhesion. *J. Biomech.* 33:23–33.